ＩＳＳＮ１３４６－７８３２

独立行政法人港湾空港技術研究所

港湾空港技術研究所報告

REPORT OF THE PORT AND AIRPORT RESEARCH INSTITUTE

VOL.49　NO.2　June 2010

NAGASE, YOKOSUKA, JAPAN

INDEPENDENT ADMINISTRATIVE INSTITUTION,
PORT AND AIRPORT RESEARCH INSTITUTE

港湾空港技術研究所報告（REPORT OF PARI）

第 49 巻　第 2 号（Vol. 49，No. 2），　2010年6月（June 2010）

目　　次（CONTENTS）

REPORT OF THE PORT AND
AIRPORT RESEARCH INSTITUTE
Vol.49, No.2 (June 2010)

Prediction of Cross-Shore Distribution of Longshore Sediment Transport Rate in and outside the Surf Zone

Yoshiaki KURIYAMA*

Synopsis

A one-dimensional model for predicting the cross-shore distribution of longshore sediment transport rate was developed. The model predicts the suspended longshore sediment transport rate due to wave breaking and bed transport rate due to longshore current velocity and velocity skewness and atiltness. The model validity was examined for transport rates due to steady flows, total longshore sediment transport rates and the cross-shore distribution of suspended longshore sediment transport rate. The model was confirmed to reproduce the longshore sediment transport rate in the field reasonably well within a factor 2 and almost completely within a factor 4. Using the developed model, longshore sediment transport rate at the Hasaki coast in Japan, where the predominant longshore current is northward near the shore and southward away from the shore, was estimated at 2-hour intervals for 15 years from 1987 to 2001. The estimated average longshore sediment transport rate is relatively small near the shore and the predominant northward sediment transport is not seen as opposed to the average longshore current velocity. Away from the shore, the average longshore sediment transport is southward and has two peaks whereas the average longshore current velocity has one. The difference is probably caused by a trough.

Key Words: longshore sediment transport, numerical model, bed load, suspended load
long-term average

* Head, Coastal Sediments and Processes Group, Marine Environment and Engineering Department
Nagase 3-1-1, Yokosuka, Kanagawa 239-0826, Japan
Phone：+81-46-844-5045 Fax：+81-46-841-9812 e-mail: kuriyama@pari.go.jp

港湾空港技術研究所報告
第 49 巻第 2 号(2010. 6)

砕波帯内外における沿岸漂砂量の岸沖分布の推定

栗山　善昭*

要　　旨

砕波帯内で卓越すると考えられる砕波によって浮遊した底質の移動と砕波帯外で支配的と考えられる底面近傍における掃流状態での底質移動の両方を考慮した沿岸漂砂量の岸沖分布推定モデルを構築した．モデルの推定精度を，流れのみの条件の下での掃流砂量，総沿岸漂砂量，および浮遊沿岸漂砂量の岸沖分布の観点から検討した結果，本モデルは，現地における沿岸漂砂量の岸沖分布を，実測値の 1/4～4 倍の範囲ではほぼ確実に，実測値の 1/2～2 倍の範囲ではおおむね推定できることが明らかとなった．続いて，上記のモデルを用いて茨城県波崎海岸における沿岸漂砂量の岸沖分布を 2 時間ごとに 15 年間分計算し，それらを平均することにより平均沿岸漂砂量の岸沖分布を求めた．その結果，波崎海岸における平均沿岸流は，岸から約 130m の地点よりも岸側の領域では北向き，それより沖では南向きの沿岸流が卓越しているのに対して，沿岸漂砂量は，岸から 160m の地点よりも岸側の領域ではその値が小さく，それより沖では南向きとなった．また，平均沿岸流速は一つのピークを持っているのに対して，平均沿岸漂砂量は二つのピークを持つ分布となった．

キーワード：沿岸漂砂量，数値モデル，浮遊砂，掃流砂，長期平均

＊ 海洋・水工部　沿岸環境研究領域　沿岸土砂管理研究チームリーダー
〒239-0826　横須賀市長瀬3-1-1　独立行政法人　港湾空港技術研究所
電話：046-844-5045　Fax：046-841-9812　　e-mail: kuriyama@pari.go.jp

CONTENTS

1. Introduction

The predominant longshore sediment transport rates, which are the transport rates averaged over long-term periods, cause long-term morphological changes, and hence understanding the predominant longshore sediment transport is essential for sediment budget analyses and effective coastal zone management.

The direction of the predominant longshore sediment transport near the shore can be detected from long-term shoreline changes around coastal structures using aerial photographs or morphological data because the predominant longshore sediment transport induces accumulation on the updrift side of a coastal structure and erosion on the downdrift side. However, because of the lack of field data and numerical simulations of longshore sediment transport rate away from the shore over long-term periods, the cross-shore variation of the long-term average longshore sediment transport rate is poorly understood although Sato (1996) suggested on the basis of longshore current field data that on the Kanazawa coast of Japan, the direction of the long-term average longshore sediment transport offshore may be opposite that near the shore.

Several models have been proposed for predicting cross-shore variations of longshore sediment transport rate (e.g., Bailard, 1981; van Rijn, 1984a, b; Watanabe, 1992), and have been validated by laboratory and field analyses (e.g., Bayram et al., 2001; van Maanen et al., 2009). However, these models have not explicitly included sediment suspension due to wave breaking. Although Katayama and Goda (1999) modeled the wave-breaking induced sediment suspension, its prediction is zero outside the surf zone, where sediments still move owing to waves and currents. Kobayashi et al. (2007) developed a model to simulate both suspended load caused by wave breaking and bed load outside the surf zone. However, the validity of their model was not examined against field data.

An objective of this study was to develop a process-based one-dimensional model of cross-shore distribution of longshore sediment transport rate by modifying the cross-shore sediment transport rate formula proposed by Kuriyama (2010b), which includes suspended and bed loads and of which the validity was confirmed with field beach profile data. The validity of the model of longshore sediment transport rate was investigated using sediment transport rates measured in the field and those estimated by formulae verified by a wide range of field and laboratory data.

The other objective was to investigate the cross-shore variation of long-term average longshore sediment transport rate in the field using the developed model. For this purpose, longshore sediment transport rate was simulated for 15 years at the Hasaki coast of Japan, where the direction of long-term average longshore current velocity varies in the cross-shore direction (Kuriyama et al., 2008).

2. Numerical model

The one-dimensional numerical model for the cross-shore distribution of longshore sediment transport rate is composed of four sub-models for wave and surface roller transformation, longshore current velocity, velocity skewness and atiltness, and beach profile change. The sub-models for wave and surface roller transformation and longshore current velocity are based on Kuriyama (2010a) and that for velocity skewness and atiltness is based on Kuriyama (2010b).

2.1 Wave and surface roller transformation

The wave and surface roller transformation sub-model estimates the cross-shore variation of the root-mean-square wave height H_{rms}, which is used in estimating longshore current velocities and sediment transport rates in the following sub-models, assuming a Rayleigh distribution as the wave height probability density function over an entire computational domain, following Thornton and Guza (1983). The energy of waves with heights larger than the breaking wave height is dissipated.

The breaking wave height is estimated with Equation (1) proposed by Seyama and Kimura (1988).

$$\frac{H_b}{h_b}=C_{br}\left[0.16\frac{L_0}{h_b}\left\{1-\exp\left[-0.8\pi\frac{h_b}{L_0}\left(1+15\tan^{4/3}\beta\right)\right]\right\}-0.96\tan\beta+0.2\right] \quad (1)$$

where H_b is the breaking wave height, h_b is the breaking water depth, C_{br} is a nondimensional coefficient, L_0 is the offshore wavelength and $\tan\beta$ is the beach slope. The nondimensional coefficient C_{br} was introduced by Kuriyama (1996) to fit Equation (1), which is based on experimental data, to field data. The beach slope is defined to be positive for water depth increasing seaward and estimated as the average slope in a

30-meter-long region of which the definition point is located at the center.

Wave energy dissipation is estimated using the periodic bore model proposed by Thornton and Guza (1983) and 20 representative wave heights raging from H_b to $3H_b$.

$$\frac{\partial E_w C_g \cos\theta}{\partial x} = \int_{H_b}^{\infty} P(H)B(H)dH$$
$$B(H) = \frac{1}{4}\rho g \frac{1}{T}\frac{(B_w H)^3}{h} \quad (2)$$

where E_w is the wave energy, C_g is the group velocity, θ is the wave direction, x is the seaward distance, $P(H)$ is the probability density of the wave height, ρ is the seawater density, g is the gravitational acceleration, T is the wave period, H is the wave height, and h is the water depth. A nondimensional parameter B_w was formulated as in Equation (3) of Kuriyama and Ozaki (1996) using Seyama and Kimura's (1988) experimental data.

$$B_w = C_B\left\{1.6 - 0.12\ln(H_0/L_0) + 0.28\ln(\tan\beta)\right\} \quad (3)$$

where H_0 is the offshore wave height and C_B is a nondimensional coefficient.

The calculation uses the peak wave period as the wave period, following Grasmeijer and Ruessink (2003). The significant wave height $H_{1/3}$ is estimated as $H_{1/3} = 1.416\ H_{rms}$.

The development and decay of surface roller in the surf zone is estimated on the basis of the energy balance as in Kuriyama (2010a), who assumes that the vertical distribution of the cross-shore velocity in a surface roller is triangular with the celerity C at the top of the roller and zero at the bottom, as described by Kuriyama and Nakatsukasa (2000).

$$\frac{\partial(E_w C_g\cos\theta)}{\partial x} + \frac{\partial(F_r\cos\theta)}{\partial x} = D_r, \quad F_r = \frac{1}{8}\rho C^3\frac{A_r}{L}$$
$$D_r = B_r\frac{gF_r}{C^2}\frac{A_r}{h^2} \quad (4)$$

where F_r is the surface roller energy flux, D_r is the energy dissipation rate of surface roller, A_r is the area of a surface roller, C is the celerity and B_r is a nondimensional coefficient, which was set to be 0.096 according to Kuriyama (2010a).

2.2 Longshore current velocity

The vertically averaged longshore current velocity V is estimated from Equation (5), which represents the momentum balance among the gradient of the radiation stress R_x, the wind stress W_x, the gradient of the momentum flux due to a surface roller M_x, and the lateral mixing term L_x and the bottom friction F_x.

$$R_x - W_x + M_x - L_x + F_x = 0 \quad (5)$$

The gradient of the radiation stress term R_x is estimated using small-amplitude wave theory.

$$R_x = \frac{1}{\rho h}\left(\frac{\partial S_{yx}}{\partial x}\right), \quad S_{yx} = \rho g\frac{C_g}{C}\frac{1}{8}H_{rms}^2\cos\theta\sin\theta \quad (6)$$

The wind stress W_x is assumed to be

$$W_x = \frac{1}{\rho h}C_d\rho_a W_v^2\sin\alpha_w \quad (7)$$

where C_d is a nondimensional coefficient (= 0.0022; Kuriyama et al., 2008), ρ_a is the air density, W_v is the wind velocity, and α_w is the wind direction.

The gradient of the momentum flux due to a surface roller M_x is expressed as

$$M_x = \frac{1}{\rho h}\left(\frac{\partial M_r}{\partial x}\right), \quad M_r = -\frac{1}{3}\rho C^2\frac{A_r}{L}\cos\theta\sin\theta \quad (8)$$

The lateral mixing term L_x is assumed, as in the study of Ruessink et al. (2001), with a dimensional coefficient N, which was set to be 0.5 m^2/s (Kuriyama, 2010a).

$$L_x = \frac{\partial}{\partial x}\left(\varepsilon\frac{\partial V}{\partial x}\right), \quad \varepsilon = \nu h \quad (9)$$

The bottom friction F_x, proposed by Nishimura (1988), is used in the model.

$$F_x = \frac{C_f}{h}\left(W + \frac{w_b^2}{W}\sin^2\theta\right)V$$
$$W = \frac{\sqrt{V^2 + w_b^2 + 2Vw_b\sin\theta} + \sqrt{V^2 + w_b^2 - 2Vw_b\sin\theta}}{2}$$
$$w_b = \frac{2v_m}{\pi}, \quad v_m = \frac{\pi H_{rms}}{T\sinh\left(\frac{2\pi h}{L}\right)} \quad (10)$$

where C_f is a nondimensional coefficient and $u_{b,rms}$ is the amplitude of orbital near-bottom velocity. Following Garcez-Faria et al. (1998) and Ruessink et al. (2001), the friction coefficient C_f is assumed to be a function of the water depth as expressed by Equation (11) with the apparent bed roughness k_a, which was set to be 0.1 m as in Kuriyama (2010a).

$$C_f = 0.015\left(\frac{k_a}{h}\right)^{1/3} \quad (11)$$

The longshore current velocity 1 m below the water surface, which will be used in the following calibration, is estimated as

$$V_z = \frac{V_*}{\kappa}\ln(\frac{z}{z_a}) \tag{12}$$

where V_* is the shear velocity, κ is the von Karman constant (= 0.4), z is the height from the bottom and z_a is the apparent roughness height, which was assumed to be $k_a/30$.

2.3 Velocity skewness and atiltness

Parameters representing the velocity and acceleration asymmetries are considered in the longshore sediment transport rate sub-model mentioned later but are not directly estimated by the wave and surface roller transformation sub-model given above. These parameters are velocity skewness $\left(\sqrt{\beta_1}\right)_u$, defined by Equation (13), and velocity atiltness $(\beta_3)_u$, proposed by Goda (1985) and defined by Equation (14).

$$\left(\sqrt{\beta_1}\right)_u = \frac{\frac{1}{N}\sum_{i=1}^{N}\left(u_i-\overline{u}\right)^3}{u_{rms}^3}, \quad u_{rms} = \frac{1}{N}\sum_{i=1}^{N}\left(u_i-\overline{u}\right)^2 \tag{13}$$

$$\left(\beta_3\right)_u = \frac{\frac{1}{N-1}\sum_{i=1}^{N-1}\left(a_i-\overline{a}\right)^3}{a_{rms}^3}, \quad a_i = \frac{u_{i+1}-u_i}{\Delta t} \tag{14}$$

$$a_{rms} = \frac{1}{N-1}\sum_{i=1}^{N-1}\left(a_i-\overline{a}\right)^2$$

where u is the fluid velocity, a is the acceleration and N is the data number. The overbar denotes the average value.

The parameters are expressed as Equations (15) and (16) using $\Pi_{1/3}$, which is a wave nonlinearity parameter proposed by Goda (1983) and defined by Equation (17), on the basis of findings of wave nonlinearity by Goda (1983), Kuriyama (1991), Doering and Bowen (1995) and Kuriyama (2010b).

$$\left(\sqrt{\beta_1}\right)_u = 0.86\Pi_{1/3}, \qquad \Pi_{1/3} < 0.15$$

$$\left(\sqrt{\beta_1}\right)_u = \left[0.54+0.90\log(\frac{3\pi}{4}\Pi_{1/3})\right] \cos\left\{\left[-90+90\tanh(0.73\frac{4}{3\pi\Pi_{1/3}})\frac{\pi}{180}\right]\right\}, \quad 0.15 \le \Pi_{1/3} \tag{15}$$

$$\left(\beta_3\right)_u = \left[-0.67-0.56\log\log(\frac{3\pi}{4}\Pi_{1/3})\right] \cos\left\{\left[-90+90\tanh(0.73\frac{4}{3\pi\Pi_{1/3}})\frac{\pi}{180}\right]\right\} \tag{16}$$

$$\Pi_{1/3} = \frac{H_{1/3}}{L_{1/3}}\coth^3\frac{2\pi h}{L_{1/3}} \tag{17}$$

where $L_{1/3}$ is the wavelength corresponding to the significant wave period.

2.4 Longshore sediment transport rate

Similar to the cross-shore sediment transport rate formula proposed by Kuriyama (2010b), the longshore sediment transport rate is assumed to consist of three contributions due to sediment suspension induced by wave breaking Q_s, near-bottom velocity $Q_{b,v}$ and near-bottom acceleration $Q_{b,a}$. The values of $Q_{b,v}$ and $Q_{b,a}$ are considered to represent the bed load.

The amount of suspended sediment is assumed to be proportional to the surface roller energy dissipation rate as in Kobayashi et al. (2008), and Q_s is expressed as

$$Q_S = \alpha_1\frac{D_r}{\rho g(s-1)w_f}V \tag{18}$$

where α_1 is a nondimensional coefficient (= 1.147 x 10^{-3}; Kuriyama, 2010b), s is the sediment specific gravity and w_f is the sediment fall velocity.

The value of $Q_{b,v}$ is assumed following Bailard (1981) as

$$Q_{b,v} = \alpha_2[(\sqrt{\beta_1})_u u_{b,rms}^3\sin\theta + u_{b,rms}^2 V(\sin^2\theta+0.5)+V^3] \tag{19}$$

where α_2 is a coefficient (= 7.651 x 10^{-4} s^2/m; Kuriyama, 2010b).

The value of $Q_{b,a}$ is expressed by Equation (20) as in the study of Hoefel and Elgar (2003).

$$Q_{b,a} = -\alpha_3\left((\beta_3)_u a_{b,rms} - a_{cr}\left|(\beta_3)_u\right|/(\beta_3)_u\right)\sin\theta, \qquad \left|(\beta_3)_u a_{b,rms}\right| > a_{cr} \tag{20}$$

$$Q_{b,a} = 0, \qquad \left|(\beta_3)_u a_{b,rms}\right| \le a_{cr}$$

where α_3 is a coefficient (= 9.960 x 10^{-5} ms; Kuriyama, 2010b), $a_{r,rms}$ is the amplitude of near-bottom acceleration and a_{cr} is a threshold value (= 0.2 m/s^2).

3. Validation of the model

Model validity was examined using transport rates due to steady flows estimated by Ribbelink's formula (1998), total longshore sediment transport rates estimated by Bayram et al.'s formula (2007) and the cross-shore distribution of suspended longshore sediment transport rate from field measurements by Miller (1998).

3.1 Transport rate due to steady flow

The validity of Equation (19) for bed load induced by near-bottom velocity was examined using Ribberink's formula (1998) for sediment transport rate due to steady flow; this formula was developed from laboratory and field data under a wide range of Shields numbers ranging from 0.01 to 10.

$$Q_R = 10.4\sqrt{(s-1)gd_{50}^3}\,(\Psi-\Psi_c)^{1.67}$$

$$\Psi = \frac{\tau_b}{(\rho_s-\rho)gd_{50}},\quad \tau_b = \rho g\frac{V^2}{C'^2}$$

$$C' = 18\log(\frac{12h}{k_s}),\quad k_s = \max\left\{3d_{90}, d_{50}\left[1+6(\Psi-1)\right]\right\} \quad (21)$$

$$\Psi_c = 0.14D_*^{-0.64},\ 4<D_*<10$$

$$D_* = d_{50}\left(\frac{g}{\nu^2}(s-1)\right)^{1/3}$$

where Q_R is the sediment transport rate estimated by Ribbelink's formula (Equation (21)), d_{50} is the median sediment diameter, d_{90} is the sediment diameter at which 90% of the sediment is finer and ν is the kinematic viscosity. Although Ribberink (1998) used both d_{50} and d_{90}, a single diameter of 0.2 mm was assumed in this study.

The model was validated with flow velocities ranging from 0.2 to 2.0 m/s at 0.2-m/s intervals and water depths from 0.5 to 7.0 m at 0.5-m intervals. **Figure 1** represents the transport rates estimated by the present model $Q_{b,v}$ and by Ribbelink's model Q_R. **Table 1** gives the root-mean-square deviation σ_{rms} defined by Equation (22) and the mean discrepancy ratios, defined as 100 minus the percentages of model estimations lying between 1/2 and 2 times Q_R and between 1/4 and 4 times Q_R (Bayram et al., 2007).

$$\sigma_{rms} = \sqrt{\frac{\Sigma\left(\log_{10}Q_{b,v} - \log_{10}Q_R\right)^2}{M-1}} \quad (22)$$

where M is the number of data.

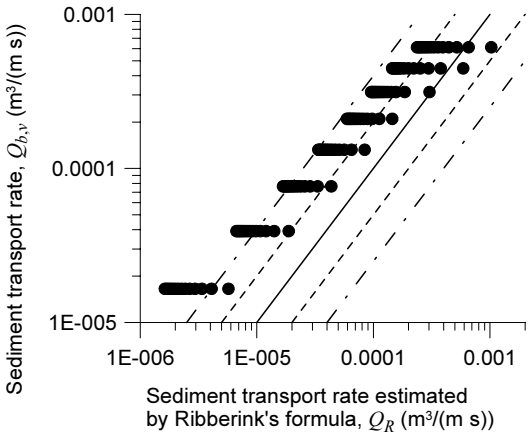

Figure 1 Comparison between Q_R and $Q_{b,v}$. The solid, broken and dot-broken lines show $Q_{b,v} = Q_R$, $Q_{b,v} = 1/2$ or 2 Q_R, and $Q_{b,v} = 1/4$ or 4 Q_R, respectively.

Table 1 Root-mean-square deviation σ_{rms} and discrepancy ratios for $Q_{b,v}$.

Q_R (m³/(ms))	Data number	σ_{rms}	$10^{\sigma rms}$	Discrepancy ratio (%) 1/2 and 2	1/4 and 4
> 0.0001	70	0.409	2.56	75.7	0.0
< 0.0001	56	1.157	14.4	98.2	73.2

The values of $Q_{b,v}$ are larger than those of Q_R (**Figure 1**), and the average $Q_{b,v}/Q_R$, $10^{\sigma rms}$, is 2.56 for $Q_{b,v}$>0.0001 m³/(m s) (**Table 1**). The percentages of $Q_{b,v}$ within a factor 2 of Q_R and a factor 4 are 24.3% and 100%, respectively, for $Q_{b,v}$>0.0001 m³/(m s).

3.2 Total longshore sediment transport rate

Total longshore sediment transport rates excluding porosity predicted by the present model were compared with those estimated by Bayram et al's formula (2007), which was based on 120 field measurements including those obtained during storms.

$$Q_{t,B} = \frac{\varepsilon}{(\rho_s-\rho)gw_f}FV_{mean}$$
$$\varepsilon = (9.0+4.0\frac{H_{1/3,b}}{w_f T})\times 10^{-5} \quad (23)$$

where $Q_{t,B}$ is the total longshore sediment transport rate estimated by Bayram et al.'s formula (2007), F is the wave energy flux before wave breaking, V_{mean} is the mean longshore current velocity in the surf zone and $H_{1/3,b}$ is the significant wave height at the wave breaking point.

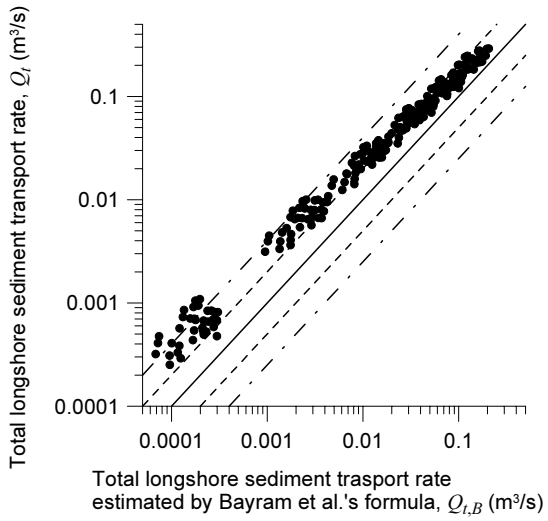

Figure 2 Comparison between $Q_{t,B}$ and Q_t. The solid, broken and dot-broken lines show $Q_t = Q_{t,B}$, Q_t = 1/2 or 2 $Q_{t,B}$, and Q_t = 1/4 or 4 $Q_{t,B}$, respectively.

Table 2 Root-mean-square deviation and discrepancy ratios for Q_t.

$Q_{t,B}$ (m³/s)	Data number	σ_{rms}	$10^{\sigma rms}$	Discrepancy ratio (%) 1/2 and 2	1/4 and 4
> 0.01	145	0.294	1.97	37.2	0.0
< 0.01	71	0.514	3.26	93.0	21.5

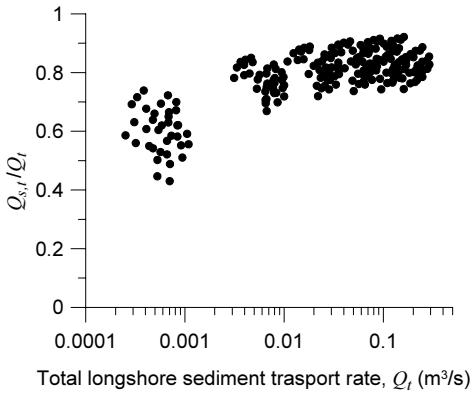

Figure 3 Ratio of suspended longshore sediment transport rate $Q_{s,t}$ to total longshore sediment transport rate Q_t.

The total longshore sediment transport rates were estimated under conditions of offshore significant wave heights from 0.5 to 3.0 m at 0.5-m intervals, wave periods from 8 to 12 s at 2-s intervals, wave directions from 10 to 40 degrees with 10-degree intervals, and beach slopes of 1/20, 1/30 and 1/50. The sediment size was assumed to be 0.2 mm.

The Q_t values estimated by the present model are slightly larger than $Q_{t,B}$ values (**Figure 2**) and the average $Q_t/Q_{t,B}$ are 1.94 for Q_t>0.01 m³/s and 3.27 for Q_t<0.01 m³/s (**Table 2**). The percentages of Q_t (>0.01 m³/s) within factors of 2 and 4 of $Q_{t,B}$ are 62.8% and 100%, respectively. The σ_{rms} values were obtained by replacing $Q_{b,v}$ and Q_R in Equation (22) with Q_t and $Q_{t,B}$, respectively.

As for the ratio of suspended and bed loads, the ratios of suspended total longshore sediment transport rate $Q_{s,t}$ to total rate Q_t are mostly 70 to 90 % and suspended load is predominant for Q_t>0.01 m³/s (**Figure 3**).

3.3 Cross-shore distribution of suspended longshore sediment transport rate

The cross-shore distribution of suspended longshore sediment transport rate estimated by Equation (18) of the present model was compared with field data obtained by Miller (1998) at Duck, North Carolina, USA, on February 4, 1998. Miller (1998) installed eight optical backscatter sensors and four electro-magnetic current meters using Sensor Insertion System from the 560-m-long pier of Field Research Facility to measure sediment fluxes. The seaward boundary was set at x = 900 m, where the water depth was about 8 m, and the grid size was 5 m. The input significant wave height was 3.8 m, peak wave period was 11.0 s, wave direction was 20.0 degrees, wind velocity was 3.3 m/s and wind direction was 74.4 degrees. The sediment diameter and fall velocity were assumed to be 0.15 mm and 0.0115 m/s, respectively. The values of C_{br} and C_B in Equations (1) and (3) were set to 1.05 and 1.10, respectively, to have minimal error between the measured and estimated significant wave heights

The estimated suspended loads are mostly smaller than the measured values (**Figure 4**) as opposed to the values estimated by the present model for transport rate due to steady flow and total longshore sediment transport rate. However, the present model reasonably reproduced the field measurement, which peaked around x = 420 m. In the surf zone, x < 450 m, the transport rates estimated with the estimated longshore current velocities are 0.22 to 1.42 times the measured transport rates and those estimated with the measured velocities are 0.42 to 1.14 times the measured rates.

3.4 Validation

The comparisons between the simulated values and field measured values or estimations by the formulae based on a wide range of data demonstrate that the present model can

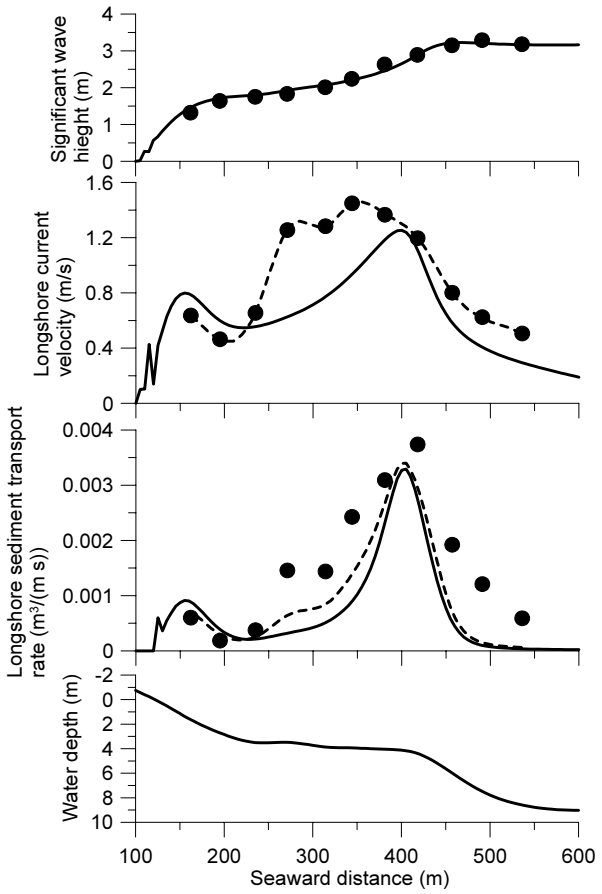

Figure 4 Cross-shore distributions of significant wave height (a), longshore current velocity (b), suspended longshore sediment transport rate (c) and elevation (d). The solid circles show measured values. The solid lines in panels (a) and (b) show estimated values, and the broken line in panel (b) show the values interpolated using the measured values and cubic spline function. The solid and broken lines in panel (c) show the values estimated with the estimated and measured longshore current velocities, respectively.

estimate the longshore sediment transport rate in the field reasonably well within a factor of 2 and almost completely within a factor of 4.

4. Estimation of cross-shore distribution of long-term average longshore sediment transport rate

At Hasaki, Japan, the direction of average longshore current velocity is northward near the shore (< 150 m) and southward away from the shore (Kuriyama et al., 2008). To examine the cross-shore distribution of the average longshore sediment transport rate under such a complex longshore current velocity field, longshore sediment transport rates at Hasaki were estimated by the present model for a 15-year period from 1987 to 2001 and the resulting characteristics were investigated.

4.1 Recalibration of longshore current velocity sub-model

Input wave parameters at the seaward boundary were wave height, period and direction. Although the input wave heights and periods were based on measured values, the input wave directions were estimated by Hashimoto et al. (2000) using WAM (WAve prediction Model), a third generation wave prediction model. Because the accuracy of the input wave direction was not high compared with accuracies of input wave height and period, a correction value for the input wave direction θ_c, giving the input wave direction as $\theta + \theta_c$, was introduced, and θ_c as well as N in Equation (9) and k_a in Equation (11), both of which affect the cross-shore distribution of longshore current velocity, was calibrated using the cross-shore distribution of the average longshore current velocity during the 15-year period from 1987 to 2001 at Hasaki.

(1) Data description

Field measurements of longshore current velocity were conducted once a weekday at intervals of about 50 m along a 427-m-long pier of the Hazaki Oceanographical Research Station (HORS), located on the Hasaki coast of Japan facing the Pacific Ocean (**Figure 5**). The nearshore current velocity 1 m below the surface was measured with a spherical float of 0.2 m diameter. The measurement method was confirmed by comparison with measurements by an electro-magnetic current meter (Kuriyama et al., 2008).

Besides the longshore current velocities, beach profiles along the pier were measured at 5-m intervals every weekday with a 5-kg lead from the pier, and with a level and staff on the shore side. The bathymetry near HORS was surveyed once or twice a year in an area 600 m wide along the shore and about 700 m long across the shore. The median sediment diameter along the profile was 0.18 mm and was almost uniform along the profile (Katoh and Yanagishima, 1995). Based on the datum level at Hasaki (Tokyo Peil -0.687 m), the high, mean and low water levels are 1.25 m, 0.65 m, and -0.20 m, respectively.

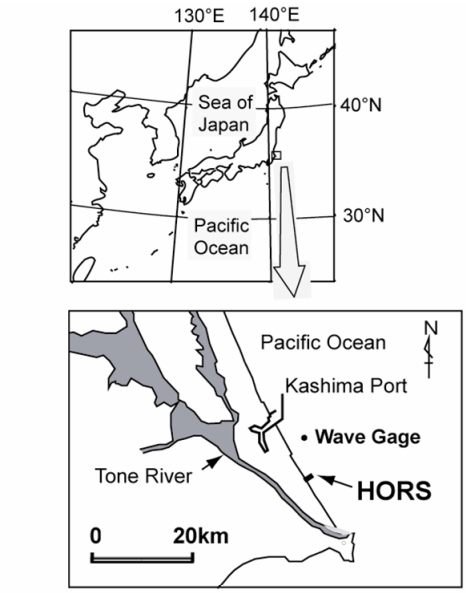

Figure 5 Locations of HORS and the wave gage.

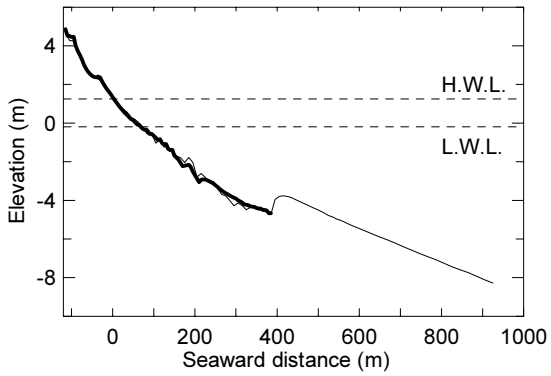

Figure 6 Mean beach profile from 1987 to 2001 based on daily measurements along the HORS pier (thick line) and yearly bathymetric surveys around HORS (thin line). The elevation is based on the Hasaki datum level.

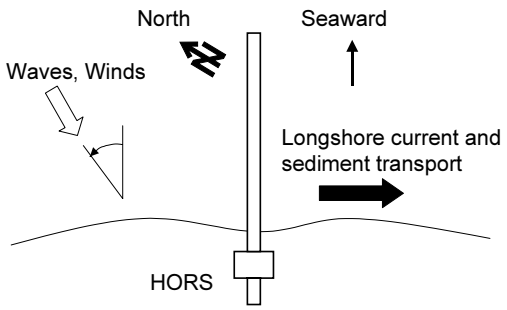

Figure 7 Coordinate system at HORS.

Figure 6 shows the mean beach profiles from 1987 to 2001. Each position along the pier is referred to by its seaward distance relative to the reference point located close to the pier entrance and designated as "P." For example, P230m denotes a position 230 m seaward from the reference point. The mean beach slope gradually decreased offshore from about 1/40 near the shoreline to about 1/100 at P300m and about 1/120 seaward of the tip of the pier. Longshore bars emerged, migrated seaward and decayed between P200m and P400m. Although local scours were observed in trough regions and the discontinuity of the averaged beach profile at P400m was probably caused by these local scours, the locations and elevations of bar crests and the locations of toughs were almost uniform alongshore (Kuriyama, 2002).

The coordinate system used in this study is shown in **Figure 7**. The positive direction of longshore current velocity and sediment transport rate was defined as being southward. The wave and wind angles were defined relative to the shoreward direction and were positive in the counterclockwise direction.

Deepwater waves were measured at approximately 24-m water depth with an ultrasonic wave gage for 20 minutes every 2 hours (**Figure 5**). Wave angles were visually observed at the tip of the pier once a weekday, although they were not used in the calibration. Wind angles and velocities were measured at the tip of the pier for 10 minutes every hour.

Deepwater wave height was large from January to March and from September to October, but small from June to August (**Figure 8 (a)**). On the other hand, the wave period was almost constant at 8 s (b). Waves came mainly from the north from December to February, and from the south from May to August (c). Strong winds came from the north from October to February, whereas weak winds came from the south from May to August (d). The yearly changes were small compared with the seasonal changes.

(2) Calibration result

The calculations of longshore current velocities for the calibration were conducted when the longshore current velocities were measured in the field, once a weekday. The cross-shore grid size was set at 10 m, and the seaward boundary was set at P1645m, where the elevation was -14.5 m relative to the Hasaki datum level. The input data at the seaward boundary were the wave heights and periods estimated from wave gage measurement at approximately

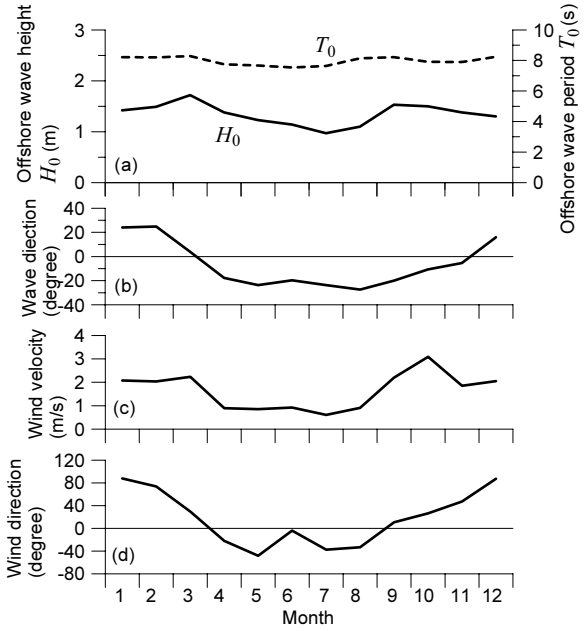

Figure 8 Monthly average offshore wave height and period (a), wave angle visually observed at the tip of the HORS pier (b), and wind velocity (c) and angle (d).

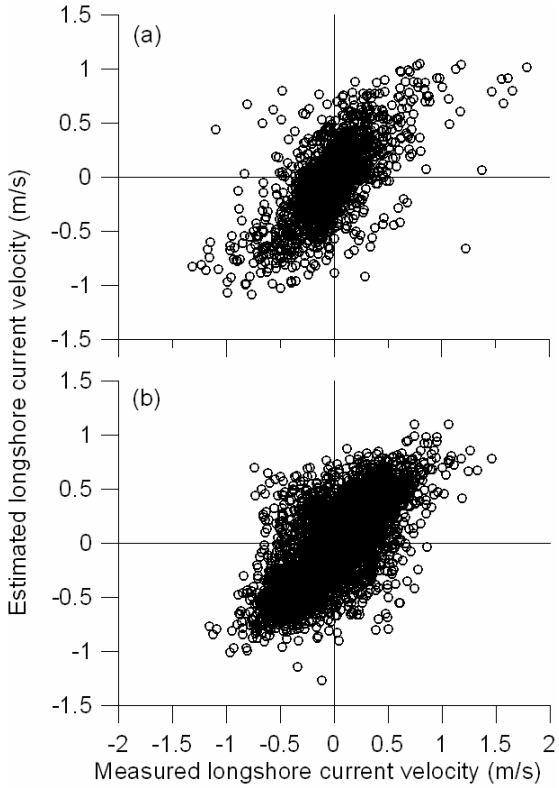

Figure 9 Comparison between measured and estimated longshore current velocities at P380m (a) and P115m (b).

24-m water depth (**Figure 5**), the wave angles estimated by WAM, and the estimated astronomical tide levels.

The initial beach profile shoreward of P385m was set as the profile measured on January 4, 1989, and that seaward of P445m was set as the mean beach profile, as shown in **Figure 6**. The profile between P390m and P440m was interpolated from the elevations at P385m and P445m.

The values of C_{br} and C_B were set to 0.70 and 0.75, respectively, to have minimal error between the measured (Kuriyama et al., 2008) and estimated significant wave heights along the HORS pier during the period from 1987 to 2001.

The parameter values of θ_c, N and k_a were determined so that the root-mean-square error of the average longshore current velocity was minimal. The resulting best parameter set was θ_c = 6 degrees, N = 5.0 m^2/s and k_a = 0.15 m. The root-mean-square errors for the average longshore current velocity and longshore current velocity are 0.0035 m/s and 0.25 m/s, respectively.

The k_a value of 0.15 m is almost the same as the k_a value of 0.1 m obtained by Kuriyama (2010a) based on field data including accurate incident wave directions. However, the N value of 5.0 m^2/s in this study is ten times the value of 0.5 m^2/s reported by Kuriyama (2010a). When N is small, the peak value is prominent and a small discrepancy of the peak location results in a large error. The large N in this study may have resulted from reducing such error by smoothing the cross-shore distribution of estimated longshore current velocity, which would have included errors caused by inaccurate wave directions.

The estimated and measured longshore current velocities have positive correlations, while there are some scatters (**Figure 9**). The cross-shore distribution of average longshore current velocity estimated by the present model with the best parameter values correlate well with the measured distribution of northward near the shore and southward away from the shore (**Figure 10**). The causes of the complex cross-shore distribution of average longshore current velocity were discussed by Kuriyama et al. (2008).

4.2 Estimation of longshore sediment transport rate

The average longshore current velocity is northward and southward shoreward and seaward of P130m, respectively. The average longshore sediment transport rate, however, is relatively small shoreward of P160m (**Figure 11**). Seaward of P160m, it is southward with two peaks around P220m and

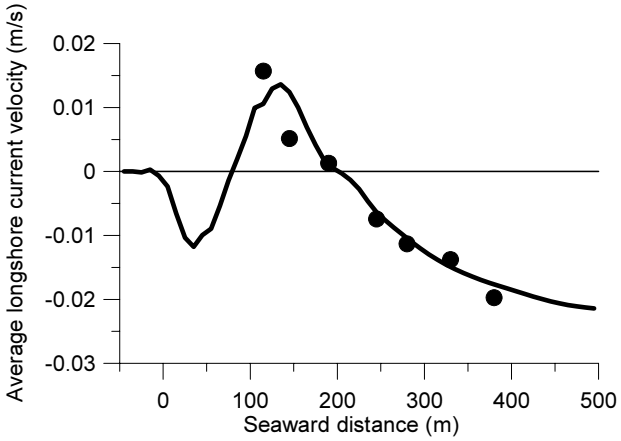

Figure 10 Average longshore current velocities measured (solid circles) and estimated (solid line).

P470m. The ratio of suspended sediment transport rate to the longshore sediment transport rate is high, as described in section 3.4, and ranges from 50% to 85%.

While the average longshore current velocity is northward near the shore, the average longshore sediment transport rate is not northward. Kuriyama et al. (2008) showed that the cross-shore distribution of average longshore current velocity is produced by the combination of the southward and northward currents. The southward current is caused by relatively high offshore waves and is thus relatively strong but also less frequent. The northward current is caused by relatively low offshore waves and is thus relatively weak but more frequent. Near the shore, although the average northward current velocity is relatively small as mentioned above, the sum of the northward current velocity prevailed over that of southward current velocity and hence the northward current is predominant.

The suspended longshore sediment transport rate, which mostly predominates over the bed transport rate, is expressed by the product of longshore current velocity and surface roller energy dissipation rate (Equation (18)). Because both are expected to be proportional to the offshore wave height, the difference between the absolute values of southward and northward longshore sediment transport rates is larger than that between southward and northward longshore current velocities. Consequently, even though the northward sediment transport occurs more frequently than the southward transport, the northward longshore sediment transport rate is not dominant near the shore.

In the region from P150m to P600m, the average longshore sediment transport rate has two peaks and is lower than 100

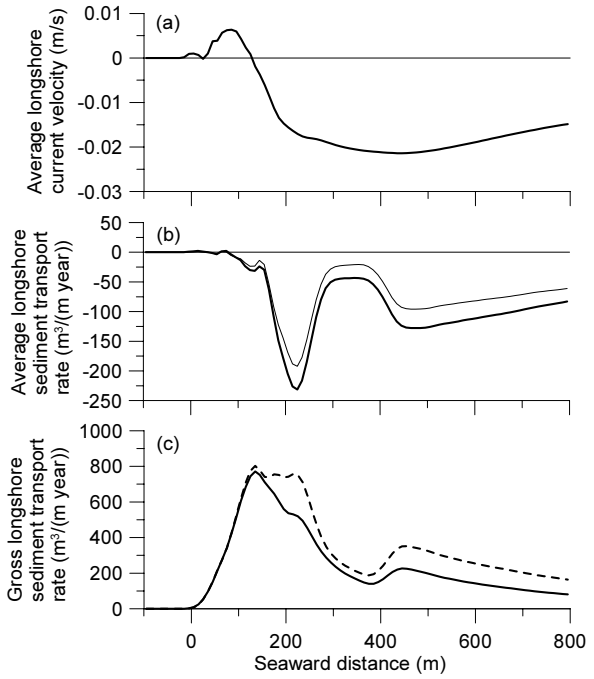

Figure 11 Cross-shore distributions of average longshore current velocity (a), average values of longshore sediment transport rate (b, thick line) and suspended longshore sediment transport rate (b, thin line), and the absolute values of northward (solid line) and southward (broken line) gross longshore sediment transport rate for a year (c).

m^3/(m s) from P260m to P420m, whereas the average longshore current velocity has only one peak. The average beach profile includes a small trough shoreward of P400m caused by local scour around piles at the tip of the pier (**Figure 6**). At a trough, although longshore current velocity is not necessarily smaller and may even be larger than at the crest (e.g., Church and Thornton, 1993; Kuriyama and Ozaki, 1993; Smith et al., 1993; Kuriyama and Nakatsukasa, 2000), the surface roller energy dissipation rate becomes smaller (e.g., Kuriyama, 2010b). Thus the longshore sediment transport rate decreased at the trough.

The average longshore current velocity illustrated in **Figure 11** does not include the near-shore southward current as shown in **Figure 10** because of the tidal levels of the current measurements. The values in **Figure 10** were obtained using the calculation results when the current measurements were conducted. The measurements were mostly conducted in the morning, when tidal levels are higher in winter than in summer. This indicates that the calculation region expanded more shoreward in winter, when the southward longshore current is predominant, than in summer, when the northward

current is predominant. Hence the predominant southward current appears in **Figure 10**. On the other hand, the average tide level in winter is almost the same as that in summer, and thus the southward current near the shore as shown in **Figure 10** does not appear in **Figure 11**, which is based on calculations at 2-hour intervals.

5. Discussion

The northward and southward gross longshore sediment transport rates integrated from the shore to a water depth of approximately 7 m, where the seaward distance is 705 m, are 28 x 10^4 and 37 x 10^4 m^3/year, respectively (**Figure 11 (c)**). These gross transport rates are smaller than the value of approximately 60 x 10^4 m^3/year for the northward and southward gross transport rates reported by Sato and Tanaka (1966), who analyzed bathymetry data obtained in 1964 and 1965. They obtained data around breakwaters and groins about 10 km north of the study site, taking measurements from the shore to approximately 7-m water depth. However, the estimated gross transport rates vary from 20 x 10^4 to 50 x 10^4 m^3/year during the 15-year period, and hence the gross transport rates of 28 x 10^4 and 37 x 10^4 m^3/year are not inconsistent with the result of Sato and Tanaka (1966).

The average longshore sediment transport rate is small and southward near the shore (**Figure 11**). Uda et al. (1986) showed that the predominant longshore sediment transport is northward at the Kashima-nada coast, which includes the Hasaki coast, on the basis of offshore wave direction data obtained with 22.5-degree resolution (16 component directions). However, Sato and Tanaka's (1966) result depicts a southward predominant longshore sediment transport. The shoreline changes detected from aerial photographs by Sato et al. (2002) showed that although the shoreline advanced from 1961 to 1984 at the northern part of the Hasaki coast, where HORS is located, owing to the construction of Kashima Port (**Figure 5**) and sand disposal south of the port, the shoreline position was stable since 1987. This result indicates that the net sediment transport rate is quite small near the shoreline and the direction of predominant longshore sediment transport is unclear, which is consistent with the result obtained in this study. Nevertheless, longshore sediment transport near the shore is more complex than assumed in the present model (e.g., Kamphius, 1991; Asano, 1996; Elfrink and Baldock, 2002; Wang et al., 2002) and further investigation and more advanced modeling of sediment transport in the swash zone are required.

6. Conclusion

A process-based one-dimensional model for predicting the cross-shore distribution of longshore sediment transport rate was developed from the cross-shore sediment transport formula developed and validated with field data by Kuriyama (2010b). The model predicts the suspended longshore sediment transport rate due to wave breaking and bed transport rate due to longshore current velocity and velocity skewness and atiltness.

The validity of the model was examined using transport rates due to steady flows estimated by Ribbelink's formula (1998), total longshore sediment transport rates estimated by Bayram et al.'s formula (2007) and the cross-shore distribution of suspended longshore sediment transport rate measured in the field by Miller (1998). The model was found to reproduce the longshore sediment transport rate in the field reasonably well within a factor of 2 and almost completely within a factor of 4.

The developed model was then used to estimate longshore sediment transport rate at the Hasaki coast, where the predominant longshore current is northward near the shore and southward away from the shore. Estimations were produced at 2-hour intervals for 15 years from 1987 to 2001, and the cross-shore distribution of the average longshore sediment transport rate was examined. The result showed that the average longshore sediment transport rate was relatively small near the shore and the predominant northward sediment transport was not seen as opposed to the average longshore current. Seaward of P160m, the average longshore sediment transport was southward with two peaks at around P220m and P470m, whereas the average longshore current velocity showed one peak. This difference in peaks was probably caused by a trough located shoreward of P400m. The longshore sediment transport rate is mainly expressed by the product of longshore current velocity and surface roller energy dissipation; the former does not decrease at a trough, whereas the latter decreases. As a result, the average longshore sediment transport rate had relatively small values at the trough shoreward of P400m, but the average longshore current did not.

(*Received on January 20, 2010*)

Acknowledgements

The author would like to thank Professor Magnus Larson, Dr. Atilla Bayram and Professor Yoshimi Goda for providing field data obtained at Duck. The offshore data were provided by the Kashima Port Construction Office of the Ministry of Land, Infrastructure, Transport and Tourism, and the Marine Information Division of the Port and Airport Research Institute. All the staff members of HORS are gratefully acknowledged for their contributions to the field measurements.

References

Asano, T. (1996): Sediment transport in swash zone under obliquely incident waves, *Proc. 25th Int. Conf. Coastal Eng.* ASCE, pp.3770-3783.

Bailard, J.A. (1981): An energetics total load sediment transport model for a planar sloping beach, *J. Geophys. Res.,* Vol.86, No.C11, pp.10938-10954.

Bayram, A., Larson, M., Miller, H.C. and Kraus, N.C. (2001): Cross-shore distribution of longshore sediment transport: comparison between predictive formulas and filed measurements, *Coastal Eng.,* Vol.44, pp.79-99.

Bayram, A., Larson, M. and Hanson, H. (2007): A new formula for the total longshore sediment transport rate, *Coastal Eng.,* Vol.54, pp.700-710.

Church, J.C., Thornton, E.B. (1993): Effects of breaking wave induced turbulence within a longshore current model, *Coastal Eng.,* Vol.20, pp.1-28.

Doering, J.C. and Bowen, A.J. (1995): Parameterization of orbital velocity asymmetries of shoaling and breaking waves using bispectral analysis, *Coastal Eng.,* Vol.26, pp.15-33.

Elfrink, B. and Baldock, T. (2002): Hydrodynamics and sediment transport in the swash zone: a review and perspectives, *Coastal Eng.,* Vol.45, pp.149-167.

Garcez-Faria, A.F., Thornton, E.B., Stanton, T.P., Soares, C.V. and Lippmann, T.C. (1998): Vertical profiles of longshore currents and related bed shear stress and bottom roughness, *J. Geophys. Res.,* Vol.103, No.C2, pp.3217-3232.

Grasmeijer, B.T. and Ruessink, B.G. (2003): Modeling of waves and currents in the nearshore parametric vs. probabilistic approach, *Coastal Eng.,* Vol.49, pp.185-207.

Hashimoto, N., Kawaguchi, K., Maki, T. and Nagai, T. (2000): A comparison of WAM and MRI based on observed directional wave spectra, *Hydrodynamics IV*, Vol. II, ICHD2000 Local Organizing Committee, pp.587-592.

Hoefel, F. and Elgar, S. (2003): Wave-induced sediment transport and sandbar migration, *Science*, Vol.299, pp.1885-1887.

Kamphuis, J.W. (1991): Alongshore sediment transport rate distribution, *Coastal Sediments '91*, ASCE, pp.170-183.

Katayama, H. and Goda, Y. (1999): Sediment suspension by random breaking waves evaluated from the CERC formula, *Coastal Sediments '99*, ASCE, pp.1019-1033.

Katoh, K. and Yanagishima, S. (1995): Changes of sand grain distribution in the surf zone, *Coastal Dynamics '95*, ASCE, pp.639-650.

Kobayashi, N., Agarwal, A. and Johnson, B.D. (2007): Longshore current and sediment transport on beaches, *J. Waterway, Port, Coastal, and Ocean Eng.,* Vol.133, No.4, doi: 10.1061/(ASCE)0733-950X(2007)133:4(296).

Kobayashi, N., Payo, A. and Schmied, L. (2008): Cross-shore suspended sand and bed load transport on beaches, *J. Geophys. Res.,* Vol.113, C07001, doi:10.1029/ 2007JC004203.

Kuriyama, Y. (1991): Investigation on cross-shore sediment transport rates and flow parameters in the surf zone using field data, *Rep. Port and Harbour Res. Inst.,* Vol.31, No.2, pp.3-58.

Kuriyama, Y. (1996): Models of wave height and fraction of breaking waves on a barred beach, *Proc. 25th Int. Conf. Coastal Eng.,* ASCE, pp.247-260.

Kuriyama, Y. (2002): Medium-term bar behavior and associated sediment transport at Hasaki, Japan, *J. Geophys. Res.,* Vol.107, No.C9, 3132, doi:10.1029/2001JC000899.

Kuriyama, Y. (2010a): One-dimensional model for undertow and longshore current velocities in the surf zone, *Rep. Port and Airport Res. Inst.,* Vol.49, No.2. (in press)

Kuriyama, Y. (2010b): Numerical simulation of cyclic seaward bar migration, *Rep. Port and Airport Res. Inst.,* Vol.49, No.2. (in press)

Kuriyama, Y. and Nakatsukasa, T. (2000): A one-dimensional model for undertow and longshore current on a barred beach, *Coastal Eng.,* Vol.40, pp.39-58.

Kuriyama, Y. and Ozaki, Y. (1993): Longshore current distribution on a bar-trough beach -Field measurements at HORF and numerical model-, *Rep. Port and Harbour Res. Inst.,* Vol.32, No.3, pp.3- 37.

Kuriyama, Y. and Ozaki, Y. (1996): Wave height and fraction

of breaking waves on a bar-trough beach-Field measurements at HORS and modeling-, *Rep. Port and Harbour Res. Inst.,* Vol.35, No.1, pp.1-38.

Kuriyama, Y., Katoh, K. and Isogami, T. (1990): Wave nonlinearity and cross-shore sediment transport rate in the vicinity of breaker zone, *Proc. Coastal Eng.,* JSCE, pp.284-260. (in Japanese)

Kuriyama, Y., Ito, Y. and Yanagishima, S. (2008): Cross-shore variation of long-term average longshore current velocity in the nearshore zone, *Continental Shelf Res.,* Vol.28, No.3, pp.491-502, doi:10.1016/j.csr.2007.10.008.

Miller, H.C. (1998): Comparison of storm longshore transport rates to predictions, *Proc. 26th Int. Conf. Coastal Eng.,* ASCE, pp.2967-2954.

Nishimura, H. (1988): Computation of nearshore current, In *Nearshore Dynamics and Coastal Process –Theory, Measurements and Predictive Models-* (edited by Horikawa, K.), pp.271-291.

Ribberink, J.S. (1998): Bed-load transport for steady flows and unsteady oscillatory flows, *Coastal Eng.,* Vol.34, pp.59-82.

Ruessink, B.G., Miles, J.R., Feddersen, F., Guza, R.T. and Elgar, S. (2001): Modeling the alongshore current on barred beaches, *J. Geophys. Res.,* Vol.106, No.C10, pp.22451-22463.

Sato, S. and Tanaka, N. (1966): Field investigation on sand drift at Port Kashima facing the Pacific Ocean, *Proc. 10th Int. Conf. Coastal Eng.,* ASCE, pp.595-614.

Sato, S. (1996): Effects of winds and breaking waves on large-scale coastal currents developed by winter storms in Japan Sea, *Coastal Eng. in Japan,* Vol.39, No.2, pp.129-144.

Seyama, A. and Kimura, A. (1988): The measured properties of irregular wave breaking and wave height change after breaking on the slope, *Proc. 21st Int. Conf. Coastal Eng.,* ASCE, pp.419-432.

Smith, J.M., Larson, M., Kraus, N.C. (1993): Longshore current on a barred beach: Field measurements and calculation, *J. Geophys. Res.,* Vol.98, No.C12, pp.22717-22731.

Thornton, E.B. and Guza, R.T. (1983): Transformation of wave height distribution, *J. Geophys. Res.,* Vol.88, No.C10, pp.5925-5938.

van Maanen, B., de Ruiter, P.J. and Ruessink, B.G. (2009): An evaluation of two alongshore transport equations with filed measurements, *Coastal Eng.,* Vol.56, pp.313-319.

van Rijn, L. (1984a): Sediment transport, Part I: bed load transport, *J. Hydraulic Eng.,* Vol.110, No.10, pp.1431-1456.

van Rijn, L. (1984b): Sediment transport, Part II: suspended load transport. *J. Hydraulic Eng.* 110(11), 1613-1641.

Wang, P., Smith, E.R. and Ebersole, B.A. (2002): Large-scale laboratory measurements of longshore sediment transport under spilling and plunging breakers, *J. Coastal Res.,* Vol.18, No.1, pp.118-135.

Watanabe, A. (1992): Total rate and distribution of longshore sand transport, *Proc. 23rd Int. Conf. Coastal Eng.,* ASCE, pp.2528-2541.

港湾空港技術研究所報告　第 49 巻第 2 号

２０１０．６

編集兼発行人　独立行政法人港湾空港技術研究所

発　行　所　独立行政法人港湾空港技術研究所
横須賀市長瀬３丁目１番１号
TEL. 046(844)5040 URL. http://www.pari.go.jp/

印　刷　所　株式会社　大　應

CONTENTS